

# PCCP

Accepted Manuscript



This is an *Accepted Manuscript*, which has been through the Royal Society of Chemistry peer review process and has been accepted for publication.

*Accepted Manuscripts* are published online shortly after acceptance, before technical editing, formatting and proof reading. Using this free service, authors can make their results available to the community, in citable form, before we publish the edited article. We will replace this *Accepted Manuscript* with the edited and formatted *Advance Article* as soon as it is available.

You can find more information about *Accepted Manuscripts* in the [Information for Authors](#).

Please note that technical editing may introduce minor changes to the text and/or graphics, which may alter content. The journal's standard [Terms & Conditions](#) and the [Ethical guidelines](#) still apply. In no event shall the Royal Society of Chemistry be held responsible for any errors or omissions in this *Accepted Manuscript* or any consequences arising from the use of any information it contains.

## Cage Effect on Conformational Preference and Photophysics in the Host-Guest Complex of Benzenediols with 18-Crown-6

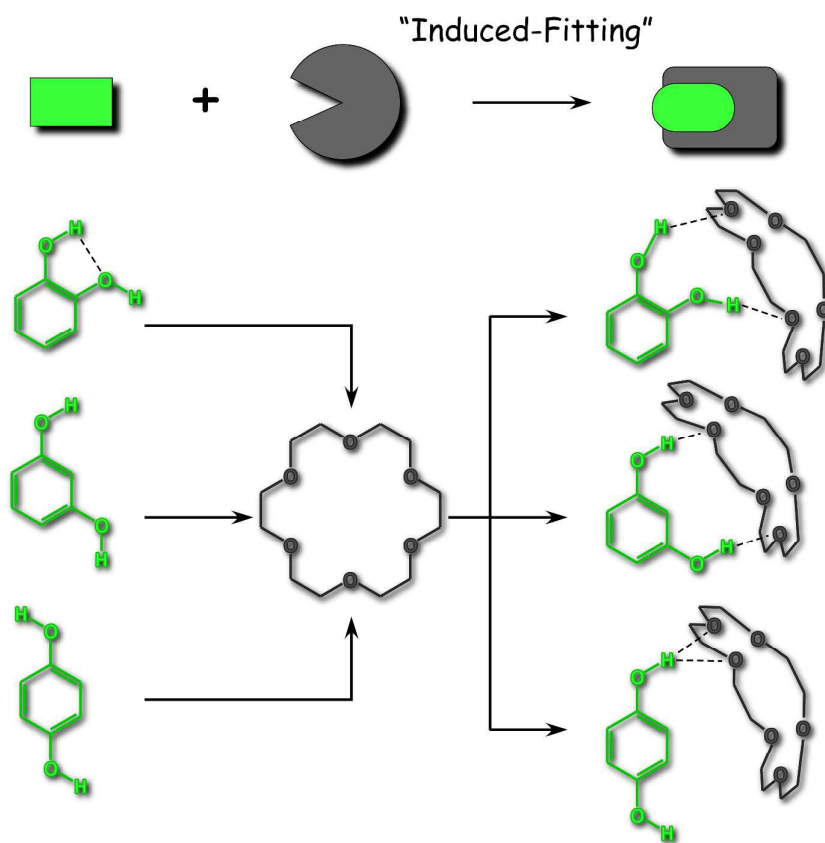
Fumiya Morishima, Ryoji Kusaka, Yoshiya Inokuchi, Takeharu Haino  
and Takayuki Ebata\*

Department of Chemistry, Graduate School of Science,  
Hiroshima University, Higashi-Hiroshima 739-8526, Japan

### Abstract

The conformational preference and modification of photophysics of benzenediols, namely hydroquinone (HQ), resorcinol (RE) and catechol (CA), upon the host-guest complex formation with 18-Crown-6 (18C6) have been investigated, under supersonically jet-cooled condition. Laser induced fluorescence (LIF) and UV-UV hole-burning spectra indicate the presence of two conformers for HQ and RE and one conformer for CA. On the other hand, the number of isomers is reduced to one in the 18C6•HQ and 18C6•RE complexes in each, while the 18C6•CA complex has three stable isomers. The IR spectra of the OH stretching vibration reveals that the two OH groups are H-bonded in 18C6•CA and 18C6•RE. In 18C6•RE, RE adopts the highest energy conformation in bare form. In 18C6•HQ, the H-bonding of one OH group affects the orientation of the other OH group. The complex formation changes the photophysics the  $S_1$  state of the benzenediols in different manner. In our previous work, we reported a remarkable  $S_1$  lifetime elongation in 18C6•CA complexes; the  $S_1$  lifetime of CA is elongated more than 1,000 times longer (8 ps  $\rightarrow$  10.3 ns) in 18C6•CA (F. Morishima et al, *J. Phys. Chem. B*, 119, 2557-2565 (2015)), which we called “cage effect”. In

18C6•RE, the increase of  $S_1$  lifetime is moderate; 4.0 ns (monomer)  $\rightarrow$  10.5 ns (complex). On the other hand, the  $S_1$  lifetime of HQ is shortened in 18C6•HQ; 2.4 ns (monomer)  $\rightarrow$  0.5 ns (complex). Density functional theory (DFT) calculations suggest that these behaviors are related to the  $S_1$  ( $^1\pi\pi^*$ ) -  $^1\pi\sigma^*$  energy gap, the character of  $S_2$  state and the symmetry of benzenediol. These experimental results clearly show the potential ability of 18C6 to control the conformation and modification of the electronic structure of guest species.



## 1. Introduction

Crown ethers (CEs) have been widely known as functionalized molecule, especially as inclusion compounds in host-guest chemistry. CE can hold cations in their cavity and are soluble in organic solvent as well as protic solvent. By using this characteristics, they are used as phase transfer catalysts. It is also known that CE exhibits a preference to encapsulate cations in bulk, depending on the size matching between the cation and CE cavity. Applications of CE as molecular receptors, metal cation extraction agents, fluoroionophores and phase transfer catalytic media have been described in a number of studies<sup>1-24</sup>. CE can include not only metal ions but also various ionic and neutral species through non-covalent interactions<sup>25-31</sup>. In our previous study, we investigated the structure of cold  $3n$ -Crown- $n$ •phenol neutral complex ( $n = 5-8$ )<sup>29</sup> and found that 18-crown-6 (18C6) and phenol form a single substantially stable 18C6•phenol 1:1 host-guest complex. 18C6 modifies its shape to be nicely matched to phenol showing “induced fit”. The structure is strongly stabilized by collective intermolecular interactions, such as OH $\cdots$ O H-bonding, CH $\cdots$  $\pi$  bonding. Furthermore, we recently studied the 18C6•catechol(CA) host-guest complex and found that 18C6 modifies not only the geometrical but also the excited state electronic structures of the guest species<sup>31</sup>, that is the  $S_1$  lifetime CA monomer, 8 ps, becomes 10.3 ns in the 18C6•CA complex. This remarkable elongation of  $S_1$  lifetime was interpreted by that 18C6 destroys the  $\pi\sigma^*$  character of the  $S_2$  state which is generally responsible for the nonradiative decay of the  $S_1$  state<sup>31</sup>.

In the present work, we extend our study to the host-guest complexes of all the benzenediols, hydroquinone (HQ), resorcinol (RE) and CA, with 18C6. We investigate their structures and the effect of the complex formation on the  $S_1$  dynamics of

benzenediols. Particularly, CA has only one stable conformation, while HQ has two and RE has three possible conformations arising from the orientation of two OH groups. We first investigate how the conformations of benzenediols and 18C6 are modified for forming the stable host-guest complex through “induced-fitting”. We then investigate how the complex formation changes the electronic structure of benzenediols by measuring their  $S_1$  lifetime. We apply various laser spectroscopic methods for the supersonically cooled molecules and complexes to measure the electronic and IR spectra. The number of conformer and isomer is determined by UV-UV hole-burning spectroscopy, and the structure of the specific isomer is investigated by IR-UV double resonance spectroscopy and quantum chemical calculations at density functional theory. The  $S_1$  state lifetime is obtained by deconvoluting the fluorescence decay profiles or the picosecond pump–probe time profiles. We will discuss how the induced-fit model can be applied for forming most stable complex structures and how the complex formation affects the excited state electronic structure of guest benzenediols.

## 2. Experimental and computational

### 2.1 Experimental

Details of the experimental setup have been described elsewhere.<sup>32</sup> The supersonic free jet of benzenediol and the 18C6•benzenediol complexes was generated by the supersonic expansion of a gaseous mixture of 18C6 and benzenediols diluted in He carrier gas (4 bar). The solid 18C6 and benzenediols samples were separately heated at different sample housings (340–370 K for 18C6, and 348, 363 and 473 K for CA, RE and HQ respectively) to be vaporized. The gas mixture was expanded into a vacuum chamber through a 1 mm orifice of a pulsed nozzle. The  $S_1$ – $S_0$  electronic spectra were observed by laser induced fluorescence (LIF) spectroscopy. A tunable UV light obtained by frequency doubling the output of Nd<sup>3+</sup>:YAG laser pumped dye laser (Lambda Physik Scanmate/Continuum Surelite II) was introduced into the vacuum chamber to be crossed with the supersonic jet at ~30 mm downstream ( $x/D = 30$ ) of the orifice. The LIF spectra were obtained by detecting the total fluorescence as a function of the UV frequency. The vibronic bands belonging to different isomers were discriminated by UV-UV hole-burning (HB) spectroscopy;<sup>33</sup> the frequency of the probe UV laser was fixed to a certain vibronic band of a specific species and its fluorescence intensity was monitored. Under this condition, another tunable UV laser (hole burning (HB) laser) pulse obtained by SHG of the Nd<sup>3+</sup>:YAG laser pumped dye laser (Continuum ND6000/Surelite II) was introduced at 10 mm upstream of the crossing point between the jet and the probe laser with a timing of ~4  $\mu$ s prior to the probe laser pulse. Then the depletion of the fluorescence intensity induced by the HB laser was monitored with scanning the frequency of UV HB laser. The UV-UV HB spectra were thus obtained as dip spectra. For IR-UV double resonance (DR) spectroscopy, the output of a pulsed

tunable OPO IR laser (Laser Vision pumped by Quanta-Ray GCR250) was employed as a HB laser. The IR laser was introduced coaxially to the probe UV pulse with an interval of 80 ns prior the UV pulse. The UV probe laser frequency was fixed to a certain vibronic band and the IR laser frequency was scanned. The depletion of the fluorescence induced by the IR pump laser was detected, giving fluorescence-dip IR spectra for the UV monitored species.

The  $S_1$  lifetimes of 18C6•CA and 18C6•RE complexes were obtained by deconvoluting the time profiles of the fluorescence decay curves by assuming the laser pulse shape as a Gaussian function with 4.5 ns pulse width. The  $S_1$  lifetimes of benzenediol monomers, H<sub>2</sub>O•HQ and 18C6•HQ complexes were too short to be determined from the fluorescence decay, so that they were obtained by pump-probe experiments with a picosecond laser system. In this experiment, the molecules or complexes in the molecular beam were ionized by stepwise two-photon ionization with two picosecond lasers. The setup of the picosecond laser system was also described in detail elsewhere.<sup>34, 35</sup> The first picosecond pump pulse excites the molecules or complexes to the  $S_1$  origin, and the second probe laser pulse ionizes the  $S_1$  state species. The ions are mass-analyzed with a 50 cm time-of-flight tube and are detected by a channeltron (Burle 4900). The ion signals were processed by a boxcar integrator (Par model 4401/4420) connected with a PC. By changing the delay time between the pump and probe lasers, the decay time profile of the  $S_1$  state was obtained. The decay time constants were determined by deconvoluting the time profiles with the 12 ps laser pulses. All the decay curves were fitted as a single exponential decay. 18C6 and all benzenediols were purchased from SIGMA-ALDRICH and NACALAI TESQUE, respectively, and used without further purification.

## 2.2 Computational

The initial structures of 18C6•benzenediol complexes were obtained by Monte Carlo simulation by mixed torsional search with low-mode sampling<sup>36</sup> in MacroModel V.9.1<sup>37</sup> with the MMFF94s force field.<sup>38</sup> The geometries were optimized by PRCG algorithm with a convergence threshold of 0.05 kJ/mol. From this calculation, 165 isomers for the 18C6•HQ, 46 isomers for 18C6•RE and 193 isomers for 18C6•CA were obtained, respectively, within 20 kJ/mol of the most stable one. All of these isomers were geometry-optimized by density functional theory (DFT) calculations at the M05-2X/6-31+G\* level with *loose* optimization criteria. This calculation yielded 5, 19, 61 isomers for 18C6•HQ, 18C6•RE and 18C6•CA, respectively, within 20 kJ/mol. These *loose*-optimized isomers were further optimized at the  $\omega$ B97X-D/6-31++G\*\* level with *tight* optimization criteria and *ultrafine* grid. The total energies were corrected by nonscaled zero-point vibrational energy (ZPE). The interaction energy ( $E_{int}$ ) of 18C6•benzenediol complexes were computed with counterpoise correction to remove the basis set superposition error (BSSE),

$$\begin{aligned}
 E_{int}(18C6 \cdots \text{benzenediol}) & \\
 &= E(18C6 \cdots \text{benzenediol}) - E(18C6) - E(\text{benzenediol}) \\
 &+ E_{BSSE}(18C6 \cdots \text{benzenediol})
 \end{aligned}
 \tag{1}$$

, where conformations of 18C6 and benzenediol fragments were fixed to the same as those in the 18C6•benzenediol complex. The IR spectra were obtained by vibrational analysis, and the vertical electronic transition energies were obtained by TD-DFT calculations at the  $\omega$ B97X-D/6-31++G\*\* level. All the DFT calculations were performed with the Gaussian 09 package, revision D.01.<sup>39</sup> The OH stretching



frequencies were scaled by 0.9346, 0.9325 and 0.9325 for HQ, RE, and CA, respectively, to reproduce the observed OH stretching vibration of each monomer. Though the calculated electronic energies are the vertical excitation energies, they are scaled by 0.8645, 0.8603 and 0.8598, for HQ, RE and CA, respectively, to reproduce the observed  $S_1$ - $S_0$  band origin energy of each monomer.

### 3. Results

#### 3.1 S<sub>1</sub>-S<sub>0</sub> spectra of benzenediols and their complexes

Fig. 1 shows the LIF and UV-UV HB spectra of the S<sub>1</sub>-S<sub>0</sub> transition of jet cooled HQ, RE, and CA and their complexes with 18C6. Fig. 1(a) shows the LIF spectrum of HQ in the S<sub>1</sub>-S<sub>0</sub> band origin region. Two strong bands at 33515 and 33550 cm<sup>-1</sup> are already assigned to the 0,0 band of two conformers of HQ, namely *trans*- and *cis*-HQ, respectively<sup>40</sup> (see Scheme 1). Weak bands at 33164 and 33201 cm<sup>-1</sup> are the band origins of H<sub>2</sub>O•HQ 1:1 complex<sup>41</sup> due to the residual water in the sample. Fig. 1(b) shows the LIF spectrum measured by adding 18C6 vapor to the gas mixture. New bands appearing around 33100-33200 cm<sup>-1</sup> can be assigned to the 18C6•HQ 1:1 complex. The UV-UV HB spectrum obtained by monitoring band A<sub>HQ</sub> is shown in Fig. 1(c). This result clearly shows that the 18C6•HQ 1:1 complex has a single isomer in spite of the fact that HQ monomer has two conformers with almost equal abundance. The ratio of the band intensity for *cis*-HQ/*trans*-HQ is 0.86 without 18C6 vapor, while it becomes 0.57 with 18C6 vapor, indicating that the relative abundance of *cis*-HQ is reduced by the addition of 18C6 and that *cis*-HQ conformer prefers the complex formation with 18C6 more than *trans*-HQ.

Fig. 1(d) and (e) exhibit the LIF spectra of RE without and with 18C6 vapor, respectively. RE monomer has three possible conformations (See Scheme 1, conformer I, II and III.). Hereafter we call these conformers RE(I), RE(II) and RE(III), respectively. The bands at 35965 and 36217 cm<sup>-1</sup> are assigned to 0,0 band of RE(I) and RE(II), respectively<sup>42</sup>. Thus, under the present jet-cooled condition, only RE(I) and RE(II) are observed in the LIF spectrum. The total energy of RE(III) is 8.86 kJ/mol higher than that of RE(I) at present level of the calculation, and the electronic transition of RE(III)

appears only under warmer jet conditions.<sup>43</sup> By the addition of 18C6 vapor, many bands due to the 18C6•RE 1:1 complex appear as seen in Fig. 1(e). The UV-UV HB spectrum in Fig. 1(f) indicates that they belong to the same isomer showing the band  $\mathbf{A}_{\text{RE}}$  (35339  $\text{cm}^{-1}$ ) as the 0,0 band. Thus, 18C6•RE 1:1 complex has only one isomer although RE monomer has three possible conformations.

Fig. 1(g) and 1(h) show the LIF spectra of CA without and with 18C6 vapor, respectively. The spectra are essentially the same as those reported in our previous paper.<sup>31</sup> The band labeled **CA** in Fig. 1(g) at 35695  $\text{cm}^{-1}$  is the 0,0 band of CA monomer. In the spectrum, the bands of H<sub>2</sub>O•CA complex also appeared. This is due to the presence of residual water in the sample. In CA, two adjacent OH groups form an intramolecular H-bond, so that it has a stable single conformer as seen in Scheme 1. The intensity of band **CA** in Fig. 1(g) is very weak due to the fast internal conversion (IC) to the  $^1\pi\sigma^*$  state. On the other hand, the band intensities of the 18C6•CA 1:1 complex in Fig. 1(h) are much stronger. The UV-UV HB spectra, not shown here, indicate that the new bands in Fig. 1(h) are attributed to vibronic bands belonging to either of three species labeled  $\mathbf{A}_{\text{CA}}\text{-C}_{\text{CA}}$ .<sup>31</sup> Thus, the 18C6•CA complex has three stable isomers, although bare CA has only one conformation. This is in contrast with the other two benzenediols, HQ and RE. The structures of the 18C6•benzenediol 1:1 complexes will be described in later section. The frequencies of the 0,0 bands of the S<sub>1</sub>-S<sub>0</sub> transition for the observed species are listed in Table 1.

### 3.2 IR spectra of benzenediols and 18C6•benzenediol complexes in the S<sub>0</sub> state

Figs. 2(a)–(i) display the IR-UV DR spectra of HQ, RE, CA and their complexes with 18C6 in the OH stretching frequency region obtained by monitoring

their 0,0 bands. For CA monomer, the position of the IR bands reported in a previous study is shown as arrows.<sup>44</sup> Table 1 also lists the observed frequencies of the OH stretching vibrations. The OH bands of *trans*- and *cis*-HQ appear at 3662 and 3663 cm<sup>-1</sup>, respectively<sup>45</sup>. In HQ, the two OH groups are symmetrically equivalent in the two conformers. So, the observed IR band is assigned to the antisymmetric OH stretching vibration in *trans*-HQ, while the symmetric and antisymmetric OH stretching vibrations is thought to be overlapped in *cis*-HQ. The IR spectrum of the 18C6•HQ complex (**A<sub>HQ</sub>**) is shown in Fig. 2(c). The bands at 3444 and 3657 cm<sup>-1</sup> are assigned to the H-bonded OH stretch and the free OH stretch, respectively. Several bands appearing at higher frequency side of the H-bonded OH are assigned to the combination bands with low frequency vibrations, probably intermolecular vibrations. Thus, in the 18C6•HQ complex, one OH group is H-bonded and the other is free from H-bond.

Figs. 2(d) and (e) show the IR spectra of the RE(I) and RE(II) monomer, respectively. In RE(II), antisymmetric OH stretch band has a stronger IR intensity, while in RE(I) two OH bands may have similar intensity because of the lower molecular symmetry. Actually, in both RE(I) and RE(II) only one OH band appeared at the same frequency at 3658 cm<sup>-1</sup> in the observed spectra<sup>45</sup>. This result indicates that the coupling between the two OH groups is very weak, which is also supported in the calculated spectra of Fig. 2(k). In the IR-UV spectrum of the 18C6•RE complex (**A<sub>RE</sub>**) (Fig. 2(f)), no free OH band is seen at ~3650 cm<sup>-1</sup> and three bands appear in the 3460-3500 cm<sup>-1</sup> region, which are assigned to the H-bonded OH. Among them, the intensity of the lowest frequency band at 3465 cm<sup>-1</sup> is strongest. Since RE has only two OH groups, the appearance of three bands means that one of the two higher frequency bands is the combination band with a low frequency intermolecular vibration.

Figs. 2(g)–(i) display the IR-UV spectra (red curves) of 18C6•CA by monitoring the intensity of bands  $A_{CA}$ ,  $B_{CA}$  and  $C_{CA}$ , and the calculated IR spectra (black curves) of the corresponding structures. Since the IR spectrum of monomer CA could not be obtained because of its weak fluorescence intensity, we adopted the reported values of the frequencies IR bands.<sup>44</sup> The IR spectrum of species  $C_{CA}$  shows a broad OH band centered at  $3281\text{ cm}^{-1}$  and sharp one at  $3507\text{ cm}^{-1}$ . The former band is assigned to the H-bonded OH with 18C6 and the latter to the intramolecular H-bonded OH band. The IR spectra of species  $A_{CA}$  and  $B_{CA}$  exhibit the OH bands at  $3350\text{--}3450\text{ cm}^{-1}$  region, indicating that the two OH groups are H-bonded with 18C6 with almost equal strength. The assignments of the OH vibrations by the comparison with the calculated ones will be given in later section.

### 3.3 $S_1$ lifetimes of the benzenediol monomers and their complexes

We then measured the  $S_1$  lifetime of each monomer and complexes. Fig. 3 shows the picosecond–pump-probe decay profiles of (a) *cis*-HQ, (d) RE(I), (e) RE(II) and (g) CA monomer, respectively. They are observed by exciting at the 0,0 band of  $S_1$ , giving the lifetime of  $2.6\pm 0.2\text{ ns}$ ,  $4.2\pm 0.3\text{ ns}$ ,  $4.5\pm 0.5\text{ ns}$ , and  $8.0\text{ ps}$ , respectively. The very short  $S_1$  lifetime of CA was investigated by Livingstone et al.<sup>46</sup> and Chatterley et al.,<sup>47</sup> and is attributed to the fast IC to the nearby  $^1\pi\sigma^*$  state, leading to an atomic hydrogen elimination of the acceptor OH ( $^b\text{OH}$  in Scheme 1). Figs. 3(c), (f), (h) and (i) display the fluorescence decay profiles of the 18C6 complexes. The change of the  $S_1$  lifetime upon the complexation is quite different for different benzenediols; in the case of HQ, the  $S_1$  lifetime of the 18C6•HQ complex ( $0.54\text{ ns}$ , Fig. 3(c)) is shorter by a factor of 5 than that of monomer. On the contrary, the lifetime of the 18C6•RE complex ( $10.5$

ns) is 2.5 times longer than RE monomer, and that of 18C6•CA complex (10.3 ns) is 1280 times longer than the CA monomer.

## 4. Discussion

### 4.1 Structure of 18C6•benzenediol 1:1 complexes

#### 4.1.1 18C6•HQ complex

As shown in Fig. 1(c), only one isomer appears for the 18C6•HQ complex. The fact that the reduction of the band intensity of *cis*-HQ upon the complex formation is larger than that of *trans*-HQ in the LIF spectrum suggests that the conformation of HQ in 18C6•HQ complex can be the *cis*-form. Figs. 4(a) and (b) show the calculated most stable structures of the 18C6•HQ complex within the energy of 10 kJ/mol. The relative energies of the isomers are also listed in Table 2. The dashed lines in Fig.4 represent the OH•••O ( $r_{\text{H}\cdots\text{O}} < 2.7 \text{ \AA}$ ) and CH••• $\pi$  ( $r_{\text{H}\cdots\pi} < 3.0 \text{ \AA}$ ) H-bonding between HQ (guest) and 18C6 (host) molecules. In these structures, one OH group is H-bonded to the oxygen atom in the ether ring and the opposite OH is free from an intermolecular H-bond. These structures well describe the observed IR spectra of the OH stretching vibrations, that is one OH is H-bonded and the other is free. An interesting point is that HQ adopts the *cis*-form in these conformers. This result is consistent with the experimental results that *cis*-HQ forms the complex more easily than *trans*-HQ. Of course, the *trans*-HQ may change to the *cis*-HQ upon the complex formation. Anyway, the conformation preference of HQ, *cis*-HQ, in 18C6•HQ becomes clear when we examine higher energy isomers. Fig. 4(c) shows the most stable 18C6•*trans*-HQ complex. This complex is 23.2 kJ/mol higher than the most stable 18C6•*cis*-HQ-I (Fig. 4(a)) so that the complex does not exist under the jet-cooled condition. The reason why HQ prefers *cis*-form in the

complex can be explained by that the complex is largely stabilized by the dipole-dipole interaction between *cis*-HQ and 18C6; *cis*-HQ has a dipole moment of 2.789 D, while that of *trans*-HQ is almost zero. In addition, though the most stable 18C6 has a planar structure ( $C_1$  symmetry) in bare form<sup>48-51</sup>, it changes the structure so that it has a dipole moment to include HQ. Thus, both the molecules cooperatively change the conformation to have dipole moments and stabilize during the process of the host-guest complex formation. Thus, the complex formation mechanism can be called as “induced-fitting”.

Fig. 2(j) shows the calculated IR spectra of bare HQ and 18C6•*cis*-HQ-I complex of Fig. 4(a). Both *trans*- and *cis*-HQ in bare form show the free OH stretching bands at 3663  $\text{cm}^{-1}$ . In the complex, the calculated IR spectrum of 18C6•*cis*-HQ-I shows the H-bonded (3420  $\text{cm}^{-1}$ ) and free (3653  $\text{cm}^{-1}$ ) OH stretching vibrations, which nicely reproduces the observed spectrum of species  $A_{\text{HQ}}$  (Fig. 2(c)). It should be noted that 18C6•*cis*-HQ-I, -II and 18C6•*trans*-HQ show very similar calculated IR spectra with each other (see Fig. S1, ESI†). Based on the relative energies and IR spectra, it is concluded that the structure of species  $A_{\text{HQ}}$  is 18C6•*cis*-HQ-I. This complex is stabilized through multiple interactions such as the OH•••O H-bond, CH••• $\pi$ , and dipole-dipole interactions. This synergetic effect is very important for the stabilization and conformer preference of this host-guest complex.

#### 4.1.2 18C6•RE complex

Figs. 5(a)–(e) show the stable isomers of the 18C6•RE complex within the energy of 10 kJ/mol. As shown in the Fig. 5, RE takes the RE(III) conformation in all isomers, which did not appear in the monomer form. Actually, the calculated energies of

R(II) and R(III) are 0.40 and 8.86 kJ/mol higher than R(I) in the monomer. In the complex, however, the lowest energy isomer having RE(I) conformation (18C6•RE(I)) is 27.1 kJ/mol higher than 18C6•RE(III)-I (See Fig. S2 (a), ESI†), and the 18C6•RE(II) isomer is not obtained as a stable structure even up to 40 kJ/mol. The stability of the 18C6•RE(III) isomer mostly comes from the formation of two OH•••O H-bondings as seen in Fig. 5. Fig. 2(k) shows the calculated IR spectra of RE(I), RE(II), 18C6•RE(III)-I and 18C6•RE(I). Similar to HQ, bare RE show only free OH stretch band. RE(I) and RE(II) have  $C_s$  and  $C_{2v}$  symmetry, respectively. The two free OH bands are overlapped with each other with equal intensity in RE(I), but in RE(II) the anti-symmetric OH stretch band appears much stronger than the symmetric OH stretch. In any case, both the symmetric and anti-symmetric OH stretches have almost the same frequency. The IR spectrum of 18C6•RE(III)-I shows two H-bonded OH stretching vibration at 3371 and 3396  $\text{cm}^{-1}$ , which reproduces the observed IR spectra of  $\mathbf{A}_{\text{RE}}$ . The IR spectrum of the 18C6•RE(I) isomer exhibits a free OH stretching vibration at  $\sim 3655 \text{ cm}^{-1}$ , which does not reproduce the observed IR spectrum of  $\mathbf{A}_{\text{RE}}$ . Thus, the observed species  $\mathbf{A}_{\text{RE}}$  is assigned to the 18C6•RE(III) isomer.

Similar to the case of HQ, multiple conformers coexist in bare form in RE, but the complexation with 18C6 controls the conformation of RE to the highest energy one (RE(III)) to form the most stable complex. In addition, 18C6 also changes its conformation so as to fit the guest species in its cavity. The complex is finally stabilized by the two OH•••O H-bondings, and CH••• $\pi$  interactions, and this synergy effect is also essential for the stabilization of the host-guest complex of crown ether.

#### 4.1.3 18C6•CA complex



The difference between CA and the other benzenediols (HQ and RE) is the presence of intramolecular H-bonding in bare CA, which leads to a unique feature of CA, such as the very short  $S_1$  lifetime compared to HQ or RE. Complexation with 18C6 largely affects this intramolecular H-bonding. Fig. 6 shows the calculated structures of 18C6•CA assignable to the observed three species,  $A_{CA}$ ,  $B_{CA}$  and  $C_{CA}$  in our previous study<sup>31</sup>. In that paper, species  $A_{CA}$  and  $B_{CA}$  were assigned to 18C6•CA-E1 (Fig. 6(b)) and 18C6•CA-E4 (Fig. 6(c)), respectively, in which the intramolecular H-bonding of CA is broken and the two OH groups are independently H-bonded to the oxygen atoms of 18C6 (We call Type-E). On the other hand, in species  $C_{CA}$  (Structure 18C6•CA-A1), CA retains its intramolecular H-bonding and its acceptor OH is H-bonded to the oxygen of 18C6 (We call Type-A). Other possible isomers of the 18C6•CA complex are shown in Fig. S2b (ESI†). The calculated IR spectra (black curves) of the three isomers of 18C6•CA are shown below the observed ones. The calculated IR spectrum of 18C6•CA-E1 shows H-bonded OH stretches at 3372 and 3429  $\text{cm}^{-1}$ , and that of 18C6•CA-E4 at 3386 and 3396  $\text{cm}^{-1}$ . In the IR spectrum of 18C6•CA-A1, an intermolecular H-bonded OH appears at 3311  $\text{cm}^{-1}$  and intramolecular H-bonded OH at 3584  $\text{cm}^{-1}$ . Though isomer 18C6•CA-A1, assigned to specie  $C_{CA}$ , is the most stable structure, the fluorescence intensity of species  $C_{CA}$  is rather weak compared to  $A_{CA}$  or  $B_{CA}$ . One of the possibilities of the weakness of this band is a smaller fluorescence quantum yield of this species than that of  $A_{CA}$  and  $B_{CA}$ . A measurement of the fluorescence lifetime of band  $C_{CA}$  was unsuccessful because of its weakness, so that it is difficult to discuss the relative abundance of the complexes.

Base on the results of the IR measurements, it is concluded that 18C6•CA complex has two types of isomers having different H-bonding structures. An important

point is that 18C6 has an ability to break the intramolecular H-bond of CA, which is connected to the drastic changes of the excited state electronic structure of guest CA, as will be discussed later.

#### 4.2 Energetics of 18C6•benzenediol 1:1 complex

As was described above, 18C6 and benzenediols form most stable host-guest complex at the expense of changing each structure to higher energy ones. In this section, we compare the energies of bare form in most stable conformations, and those of the distorted one for forming the complex, and that of the complex. Figs. 7(a) and (b) show the schematic energy diagram of the 18C6•HQ and 18C6•RE systems; the most stable structures of benzenediols and 18C6 (left), distorted structures (middle), and the stable 18C6•benzenediol complexes (right). It should be noted that in the figures the horizontal axis does not mean the complex formation coordinate. In Fig. 7,  $\Delta E_{CE}$  is the energy difference of 18C6 between the most stable structure in bare form and that in the complex.  $\Delta E_{HQ, RE \text{ or } CA}$  is also the energy difference of benzenediol part.  $E_{int}$  is the interaction energy of the complex,<sup>29</sup> which is obtained by using eq. (1) described in the computational section. In the 18C6•HQ-I complex,  $E_{int}$  is obtained to be 94.3 kJ/mol. In case of HQ (Fig. 7(a)), the most stable structure of bare HQ has the *trans* form. The energy difference between “most stable *trans*-HQ monomer + most stable 18C6” and 18C6•HQ-I complex corresponds to the *Binding energy* of the 18C6•HQ-I complex. In the complex, the 18C6 and HQ components takes higher energy structures, (18C6)<sup>‡</sup> and (HQ)<sup>‡</sup> (middle in Fig. 7(a)), to form the stable complex (right in Fig. 7(a)). The energy necessary for this distortion, ( $\Delta E_{CE} + \Delta E_{HQ}$ ), is 10.6 kJ/mol. Hence, the interaction energy  $E_{int}$  is represented by using the *Binding energy* and ( $\Delta E_{CE} + \Delta E_{HQ}$ ), as follows,

$$E_{\text{int}} = \text{Binding energy} + (\Delta E_{\text{CE}} + \Delta E_{\text{HQ or RE or CA}}). \quad (2)$$

The BSSE corrected *Binding energy* of the complex is obtained to be 83.7 kJ/mol. This value leads  $E_{\text{int}}$  to be 94.3 kJ/mol by using eq. (2), which is equal to that obtained by using eq. (1). Fig. 7(b) shows the schematic energy diagram for the 18C6•RE complex. The energy difference between most stable monomers and distorted ones,  $(\Delta E_{\text{CE}} + \Delta E_{\text{RE}})$ , is 31.4 kJ/mol, the *Binding energy* of the complex is 81.6 kJ/mol, and the interaction energy  $E_{\text{int}}$  is 113 kJ/mol.

Fig. 8 shows a similar energy diagram for the 18C6•CA complex system. In this case, two different types of the stable complexes are formed, 18C6•CA-A1 and 18C6•E1 as were described previously. The value of  $(\Delta E_{\text{CE}} + \Delta E_{\text{CA}})$  is 12.5 kJ/mol for 18C6•CA-A1 and 17.3 kJ/mol for 18C6•CA-E1. The *Binding energy* of the complex is 75.8 for 18C6•CA-A1 and 79.7 kJ/mol for 18C6•CA-E1, and  $E_{\text{int}}$  is 92.1 kJ/mol for 18C6•CA-A1 and 93.2 kJ/mol for 18C6•CA-E1. Table 2 lists the relative energies of the complexes ( $\Delta E$ ),  $E_{\text{int}}$ ,  $\Delta E_{\text{CE}}$ ,  $\Delta E_{\text{HQ}}$ ,  $\Delta E_{\text{RE}}$  and  $\Delta E_{\text{CA}}$  and the dihedral angles of OH groups (<sup>a</sup>OH, <sup>b</sup>OH) with respect to benzene plane. For the benzenediol part,  $\Delta E_{\text{HQ}}$  is 1.64–2.11 kJ/mol,  $\Delta E_{\text{RE}}$  is 10.6–12.9 kJ/mol, and  $\Delta E_{\text{CA}}$  is 2.28–16.2 kJ/mol. These values are quite different for different species and conformations. As seen in Figs. 7 and 8 and Table 2, all the necessary energies for forming the higher energy conformations are easily compensated by the large interaction energy of 90–110 kJ/mol or the *Binding energies* as 83.7 kJ/mol for 18C6•*cis*-HQ-I, 81.6 kJ/mol for 18C6•RE(III)-I and 70.7–79.6 kJ/mol for 18C6•CA complexes. These binding energies are roughly 4 times larger than the normal OH•••O H-bond energy (for example the H-bond energy of water dimer is 19–20 kJ/mol).<sup>52</sup> Such a large binding energy comes from the multiple interactions between benzenediols and 18C6, such as OH•••O H-bond, CH••• $\pi$  and

dipole-dipole interactions. These interactions are actually seen in the calculated structures in Figs. 4–6. In these figures, the number of OH...O and CH... $\pi$  bonding are also shown; the most stable isomers have the largest number of intermolecular bonding between the host and guest molecules. These results strongly indicate that the 18C6•benzendiol host-guest complex formation is not described as a simple rigid “lock-and-key” model, but as a flexible “induced-fit” model, like an enzyme-substrate fitting.

#### 4.3 The $S_1$ lifetime of 18C6•benzendiol complex

The observed  $S_1$  lifetime of benzenediols and 18C6•benzendiol complexes are also listed in Table 1. As was described in the Introduction section, the major non-radiative pathway of the  $S_1$  state of benzenediols is thought to be IC to  $S_2$  ( $\pi\sigma^*$ ) via the conical intersection, following by the O–H bond fission along the repulsive  $S_2$  potential curve or the further IC to  $S_0$  via the  $S_2 - S_0$  conical intersection. Anomalous short lifetime of bare CA (8 ps) is described by the low barrier height of  $S_1 - S_2$  conical intersection due to the small  $S_1/S_2$  energy gap ( $\Delta E_{2-1}$ ) and low symmetry ( $C_1$ ) in the  $S_1$  state.<sup>53, 54</sup> So, we calculated the vertical excitation energies to the  $S_1$  and  $S_2$  states with the fixed  $S_0$  geometry and obtained the  $S_1$ - $S_2$  energy gap  $\Delta E_{2-1}$ , which is also listed in Table 1. Since we do not calculate the potential energies curves along the O --- H coordinate,  $\Delta E_{2-1}$  is not equal to the barrier height at the  $S_1 - S_2(\pi\sigma^*)$  conical intersection. Even if it is so, we consider that this value is roughly proportional to the barrier height. The calculated  $\Delta E_{2-1}$  of bare HQ and RE are 0.439–0.571 eV, while that of CA is much smaller, 0.256 eV. This difference is in good agreement with the shorter  $S_1$  lifetime of CA than HQ or RE. The complex formation with 18C6 greatly affects

the nonradiative process of each benzenediol in different manners. First, in the case of HQ, the  $S_1$  lifetime is shortened by a factor of five (2.8 ns  $\rightarrow$  0.54 ns) in the complex, while the lifetime is 2.5 times lengthened in the RE complex (4.0 ns  $\rightarrow$  10.5 ns) and 1280 times in the type-E complex of CA (8.0 ps  $\rightarrow$  10.3 ns). Thus, the 18C6•HQ complex shows an opposite trend of the  $S_1$  lifetime behavior compared to that of 18C6•RE and 18C6•CA. This difference is attributed to the presence of free OH in 18C6•HQ but not in 18C6•RE and 18C6•CA. As seen in Table 1, The presence of free OH does not affect strongly the  $\Delta E_{2-1}$  value: 0.471 eV for RE(I) changes to 0.512 eV for 18C6•RE(III)-I and 0.488 eV for *cis*-HQ changes to 0.496 eV for 18C6•HQ-II. Only CA shows large change of  $\Delta E_{2-1}$  value upon the complex formation: 0.256 eV for CA  $\rightarrow$  0.721 eV for 18C6•CA-E1. However, the difference can be seen clearly in the molecular orbitals of the electronic states between 18C6•HQ, 18C6•RE and 18C6•CA. The molecular orbitals responsible for the  $S_1$  and  $S_2$  electronic states are shown in Fig. S3 (ESI†). In the figures, it is clear that the  $\sigma^*$  character dominates in the  $S_2$  state in all the monomer species. On the other hand, for the 18C6 complexes, the  $\sigma^*$  character can be seen only at the free OH site of 18C6•HQ (Fig. S3(c), ESI†). In addition, the dihedral angle defined in Scheme 1 of *cis*-HQ becomes 168–178 degree, indicating that the molecular symmetry of *cis*-HQ becomes lower from  $C_{2h}$  to  $C_1$  by the complexation. Hence, this lower molecular symmetry causes the shorter  $S_1$  lifetime of HQ upon the complexation. In case of 18C6•RE and 18C6•CA, the cage of 18C6 diminishes the  $\sigma^*$  character in the  $S_2$  state, leading to the suppression of the OH cleavage. Rizzo and co-workers observed similar lifetime elongation in protonated tryptophan-(H<sub>2</sub>O)<sub>2</sub> complex<sup>55</sup>. The protonation to tryptophan lowers the energy of the  $\pi\sigma^*$  ( $\sigma^*$  of N-H) state, facilitating a mixing between the  $\pi\sigma^*$  and indole  $\pi\pi^*$  states. Thus, the protonated

tryptophan monomer exhibits very broad electronic spectrum. In contrast, the hydration to the  $\text{NH}_3^+$  group by two water molecules shifts the  $\sigma^*$  of N-H to higher energy and resulting in the decoupling of  $\pi\sigma^*$  from  $\pi\pi^*$ . In other words, two water molecules “block” the N-H bond fission of protonated tryptophan in excited state, resulting in the sharp electronic spectrum. In the case of  $18\text{C}6\cdot\text{HQ}$ , the  $\pi\sigma^*$  character is still retained in the free OH group in the  $\text{S}_2$  state as seen Fig. S3(e) (ESI†).

## 5. Conclusion

In the present study, we investigated the formation of host-guest complexes between  $18\text{C}6$  and benzenediols in the gas phase under the supersonically jet-cooled condition. We found that  $18\text{C}6$  and benzenediols cooperatively changes their conformations from the stable bare forms to higher energy ones for the best-fitted stable complexes. The complexes are stabilized synergistically through multiple interactions. Especially, the RE part in  $18\text{C}6\cdot\text{RE}$  takes the characteristic conformation (RE(III)), which is the highest energy one in monomer form. In the  $18\text{C}6\cdot\text{CA}$  type-E complex, CA breaks its intramolecular H-bond to form two intermolecular H-bonds with  $18\text{C}6$ . It is also found that complex formation controls the direction of the OH group remote from the direct contact. All the complexes are stabilized by synergetic intermolecular interactions, which are produced by the geometry changes of the host and guest species via typical “induced-fit” mechanism.

It was also found that the host-guest complexation with crown ethers drastically change the electronic excited state of guest species. In case of RE and CA,

the  $S_1$  lifetime is lengthened by a factor of 2.5 and 1280, respectively. This drastic change is described by partly an increase of  $S_1/S_2$  energy gap and mostly destruction of the  $\pi\sigma^*$  character of the  $S_2$  state. On the contrary, in HQ, the complexation shortens the  $S_1$  lifetime of HQ by a factor of five, thus accelerating the nonradiative decay rate. The present study has shown that 18C6, simple crown ether, can exert the isomeric preference and modify the excited state dynamics of guest species through multiple interactions. As a future work, we will extend this work to more flexible molecule as a guest and elucidate the potential ability of crown ether as a control of conformer preference as well as the excited state dynamics of the guest.

#### **Acknowledgment**

T. E. acknowledges Japan Society for the Promotion (JSPS) for the support through a Grand-in-Aid project (No. 25410017).

**References**

1. C. J. Pedersen, *J. Am. Chem. Soc.*, 1967, **89**, 7017–7036.
2. C. J. Pedersen, H. K. Frensdorff, *Angew. Chem. Int. Ed. Engl.*, 1972, **11**, 16–25.
3. C. J. Pedersen, *Science* 1988, **241**, 536–540.
4. R. M. Izatt, J. H. Rytting, D. P. Nelson, B. L. Haymore, J. J. Christensen, *Science* 1969, **164**, 443–444.
5. R. M. Izatt, D. P. Nelson, J. H. Rytting, J. J. Christensen, *J. Am. Chem. Soc.*, 1971, **93**, 1619–1623.
6. R. M. Izatt, R. E. Terry, B. L. Haymore, L. D. Hansen, N. K. Dalley, A. G. Avondet, J. J. Christensen, *J. Am. Chem. Soc.*, 1976, **98**, 7620–7626.
7. R. M. Izatt, R. E. Terry, D. P. Nelson, Y. Chan, D. J. Eatough, J. S. Bradshaw, L. D. Hansen, J. J. Christensen, *J. Am. Chem. Soc.*, 1976, **98**, 7626–7630.
8. J. D. Lamb, R. M. Izatt, C. S. Swain, J. J. Christensen, *J. Am. Chem. Soc.*, 1980, **102**, 475–479.
9. H. Zhang, J. H. Chu, S. Leming, D. V. Dearden, *J. Am. Chem. Soc.*, 1991, **113**, 7415–7417.
10. H. Zhang, D. V. Dearden, *J. Am. Chem. Soc.*, 1992, **114**, 2754–2755.
11. S. Maleknia, J. Brodbelt, *J. Am. Chem. Soc.*, 1992, **114**, 4295–4298.
12. I. H. Chu, H. Zhang, D. V. Dearden, *J. Am. Chem. Soc.*, 1993, **115**, 5736–5744.
13. L. X. Dang, *J. Am. Chem. Soc.*, 1995, **117**, 6954–6960.
14. P. D. J. Grootenhuis, P. A. Kollman, *J. Am. Chem. Soc.*, 1989, **111**, 2152–2158.
15. D. Ray, D. Feller, M. B. More, E. D. Glendening, P. B. Armentrout, *J. Phys. Chem.*, 1996, **100**, 16116–16125.
16. F. Sobott, W. Kleinekofort, B. Brutschy, *Anal. Chem.*, 1997, **69**, 3587–3594.
17. M. B. More, D. Ray, P. B. Armentrout, *J. Phys. Chem. A*, 1997, **101**, 4254–4262.



18. M. B. More, D. Ray, P. B. Armentrout, *J. Phys. Chem. A*, 1997, **101**, 7007–7017.
19. M. B. More, D. Ray, P. B. Armentrout, *J. Am. Chem. Soc.*, 1999, **121**, 417–423.
20. Y. Inokuchi, O. V. Boyarkin, R. Kusaka, T. Haino, T. Ebata, T. R. Rizzo, *J. Am. Chem. Soc.*, 2011, **133**, 12256-12263.
21. Y. Inokuchi, O. V. Boyarkin, R. Kusaka, T. Haino, T. Ebata, T. R. Rizzo, *J. Phys. Chem. A*, 2012, **116**, 4057-4068.
22. Y. Inokuchi, R. Kusaka, T. Ebata, O. V. Boyarkin, T. R. Rizzo *ChemPhysChem.*, 2013, **14**, 649-660.
23. Y. Inokuchi, T. Mizuuchi, T. Ebata, T. Ikeda, T. Haino, T. Kimura, H. Guo, Y. Furutani, *J. Am. Chem. Soc.*, 2014, **592**, 90-95.
24. Y. Inokuchi, T. Ebata, T. R. Rizzo, O. V. Boyarkin, *Chem. Phys. Lett.*, 2014, **136**, 1815-1824.
25. R. Kusaka, Y. Inokuchi, T. Ebata, *Phys. Chem. Chem. Phys.*, 2007, **9**, 4452-4459.
26. R. Kusaka, Y. Inokuchi, T. Ebata, *Phys. Chem. Chem. Phys.*, 2008, **10**, 6238-6244
27. R. Kusaka, Y. Inokuchi, T. Ebata, *Phys. Chem. Chem. Phys.*, 2009, **11**, 9132-9140.
28. S. Kokubu, R. Kusaka, Y. Inokuchi, T. Haino, T. Ebata, *Phys. Chem. Chem. Phys.*, 2010, **12**, 3559-3565.
29. R. Kusaka, Y. Inokuchi, T. Haino, T. Ebata, *J. Phys. Chem. Letters*, 2012, **3**, 1414-1420.
30. Y. Inokuchi, O. V. Boyarkin, T. Ebata, T. R. Rizzo, *Phys. Chem. Chem. Phys.*, 2012, **14**, 4457-4462.
31. F. Morishima, R. Kusaka, Y. Inokuchi, T. Haino, T. Ebata, *J. Phys. Chem. B*, 2015, **119**, 2557-2565.
32. Y. Inokuchi, Y. Kobayashi, T. Ito, T. Ebata, *J. Phys. Chem. A* 2007, **111**, 3209–3215.
33. R. J. Lipert, S. D. Colson, *J. Phys. Chem.*, 1989, **93**, 3894–3896.

34. Y. Yamada, N. Mikami, T. Ebata, *Proc. Natl. Acad. Sci. U. S. A.*, 2008, **105**, 12690–12695.
35. R. Kusaka, T. Ebata, *Angew. Chem., Int. Ed.*, 2010, **49**, 6989–6992
36. I. Kolossváry, W. C. Guida, *J. Am. Chem. Soc.*, 1996, **118**, 5011–5019.
37. MacroModel, version 9.1; Schrödinger, LLC: New York, 2005.
38. T. A. Halgren, *J. Comput. Chem.*, 1999, **20**, 730–748.
39. Gaussian 09, Revision D.01, M. J. Frisch, G. W. Trucks, H. B. Schlegel, G. E. Scuseria, M. A. Robb, J. R. Cheeseman, G. Scalmani, V. Barone, B. Mennucci, G. A. Petersson, H. Nakatsuji, M. Caricato, X. Li, H. P. Hratchian, A. F. Izmaylov, J. Bloino, G. Zheng, J. L. Sonnenberg, M. Hada, M. Ehara, K. Toyota, R. Fukuda, J. Hasegawa, M. Ishida, T. Nakajima, Y. Honda, O. Kitao, H. Nakai, T. Vreven, J. A. Montgomery, Jr., J. E. Peralta, F. Ogliaro, M. Bearpark, J. J. Heyd, E. Brothers, K. N. Kudin, V. N. Staroverov, R. Kobayashi, J. Normand, K. Raghavachari, A. Rendell, J. C. Burant, S. S. Iyengar, J. Tomasi, M. Cossi, N. Rega, J. M. Millam, M. Klene, J. E. Knox, J. B. Cross, V. Bakken, C. Adamo, J. Jaramillo, R. Gomperts, R. E. Stratmann, O. Yazyev, A. J. Austin, R. Cammi, C. Pomelli, J. W. Ochterski, R. L. Martin, K. Morokuma, V. G. Zakrzewski, G. A. Voth, P. Salvador, J. J. Dannenberg, S. Dapprich, A. D. Daniels, Ö. Farkas, J. B. Foresman, J. V. Ortiz, J. Cioslowski, and D. J. Fox, Gaussian, Inc., Wallingford CT, 2009.
40. S. J. Humphrey, D. W. Pratt, *J. Chem. Phys.*, 1993, **99**, 5078.; *J. Chem. Phys.*, 1996, **104**, 2752.;
41. P. S. Meenakshi, N. Biswasa, S. Wategaonkar, *Phys. Chem. Chem. Phys.*, 2003, **5**, 294–299.
42. M. Gerhards, W. Perl, K. Kleinermanns, *Chem. Phys. Lett.*, 1995, **240**, 506–512.

43. S. Melandri, G. Maccaferri, W. Caminati, P. G. Favero, *Chem. Phys. Lett.*, 1996, **256**, 513-517
44. M. Gerhards, C. Unterberg, K. Kleinermanns, *Phys. Chem. Chem. Phys.*, 2000, **2**, 5538–5544.
45. K. Hattori, S. Ishiuchi, *J. Phys. Chem. A*, 2007, **111**, 6028-6033
46. R. A. Livingstone, J. O. F. Thompson, M. Iljina, R. J. Donaldson, B. J. Sussman, M. J. Paterson, D. Townsend, *J. Chem. Phys.*, 2012, **137**, 184304
47. A. S. Chatterley, J. D. Young, D. Townsend, J. M. Žurek, M. J. Paterson, G. M. Roberts, V. G. Stavros, *Phys. Chem. Chem. Phys.*, 2013, **15**, 6879-6892
48. G. Wipff, P. Weiner, P. Kollman, *J. Am. Chem. Soc.*, 1982, **104**, 3249–3258.
49. Y. Sun, P. A. Kollman, *J. Chem. Phys.*, 1992, **97**, 5108.
50. E. D. Glendening, D. Feller, M. A. Thompson, *J. Am. Chem. Soc.*, 1994, **116**, 10657-10669.
51. M. J. Bovill, D. J. Chadwick, I. O. Sutherland, D. Watkin, *J. Chem. Soc., Perkin Trans. 2*, 1980, 1529-1543.
52. M. W. Feyereisen, D. Feller, D. A. Dixon, *J. Phys. Chem.*, 1996, **100**, 2993-2997.
53. (a) M. Gerhards, C. Unterberg, S. Schumm, *J. Chem. Phys.* 1999, **111**, 7966. (b) W. B. Tzeng, K. Narayanan, C.Y. Hsieh, C.C. Tung, *Spectrochimica Acta Part A*, 1997, **53**, 2595–2604. (c) S. J. Humphrey, D. W. Pratt, *J. Chem. Phys.*, 1993, **99**, 5078. (d) G. A. King, T. A. A. Oliver, R. N. Dixon, M. N. R. Ashfold, *Phys. Chem. Chem. Phys.*, 2012, **14**, 3338-3345.
54. M. Weiler, M. Miyazaki, G. Féraud, S. Ishiuchi, C. Dedonder, C. Jouvét, M. Fujii, *J. Phys. Chem. Lett.* 2013, **4**, 3819–3823.

55. S. R. Mercier, O. V. Boyarkin, A. Kamariotis, M. Guglielmi, I. Tavernelli, M. Cascella, U. Rothlisberger, T. R. Rizzo, *J. Am. Chem. Soc.*, 2006, **128**, 16938–16943.

## Footnote

† Electronic supplementary information (ESI) available: See DOI: xx.xxxx/xxxxxxxxxx

Table 1 Observed and calculated frequencies of the OH stretching vibrations, observed  $S_1$ - $S_0$  transition energy, calculated vertical  $S_1$ - $S_0$  and  $S_2$ - $S_0$  transition energies and oscillator strengths,  $S_2 - S_1$  energy gap ( $\Delta E_{2-1}$ ), observed  $S_1$  lifetime and molecular symmetry of each species. The calculations are performed at the  $\omega$ B97X-D/6-31++G\*\* level.

	Band labeling	OH stretching freq.[ $\text{cm}^{-1}$ ]		$S_1$ - $S_0$ transition energy [ $\text{cm}^{-1}$ (eV)]	<sup>a</sup> Excitation energy [eV] and oscillator strength		$\Delta E_{2-1}$ [eV]	$S_1$ Lifetime [ns]	Symmetry in $S_0$	<sup>b</sup> Symmetry in $S_1$
		Obs.	Calc.		$S_1$	$S_2$				
<i>cis</i> -HQ	-	3663	3662, 3663	33550 (4.160)	4.161(0.0706)	4.649(0.0000)	0.488	2.8	$C_{2h}$	$C_{2h}$
<i>trans</i> -HQ	-	3662	3663	33515 (4.156)	4.155(0.0715)	4.726(0.0000)	0.571		$C_{2v}$	$C_{2v}$
$H_2O$ • <i>cis</i> -HQ	-	-	-	33201 (4.117)	4.112(0.0726)	4.455(0.0000)	0.343	1.2	$C_s$	-
$H_2O$ • <i>trans</i> -HQ	-	-	-	33164 (4.106)	4.108(0.0727)	4.510(0.0000)	0.402		$C_1$	-
18C6• <i>cis</i> -HQ-I	$A_{HQ}$	3444, 3657	3420, 3653	33115 (4.106)	4.092(0.0740)	4.588(0.0005)	0.496	0.54	$C_1$	-
18C6• <i>cis</i> -HQ-II	-	-	3410, 3628	-	4.104(0.0729)	4.758(0.0045)	0.654		$C_s$	$C_s$
RE(I)	-	3658	3656, 3658	35965 (4.460)	4.465(0.0363)	4.936(0.0007)	0.471	4	$C_s$	$C_s$
RE(II)	-	3658	3659	36217 (4.491)	4.484(0.0257)	4.923(0.0000)	0.439		$C_{2h}$	$C_{2h}$
RE(III)	-	-	-	-	4.425(0.0482)	4.894(0.0000)	0.469	-	$C_{2h}$	-
18C6•RE(III)-I	$A_{RE}$	3465	3371, 3396	35339 (4.382)	4.368(0.0316)	4.880(0.0008)	0.512	10.5	$C_1$	-
18C6•RE(III)-II	-	-	3359, 3401	-	4.343(0.0381)	4.968(0.0008)	0.625		-	$C_1$
18C6•RE(III)-III	-	-	3391, 3429	-	4.371(0.0365)	4.843(0.0000)	0.472	-	$C_1$	-
18C6•RE(III)-IV	-	-	3358, 3369	-	4.359(0.0417)	4.838(0.0000)	0.479	-	$C_1$	-
18C6•RE(III)-V	-	-	3412, 3462	-	4.398(0.0376)	4.939(0.0001)	0.541	-	$C_1$	-
CA	-	3611, 3673	3612, 3672	35695 (4.426)	4.426(0.0507)	4.682(0.0004)	0.256	0.008	$C_s$	$C_1$
18C6•CA-A1	$C_{CA}$	3281, 3507	3311, 3584	35397 (4.389)	4.347(0.0422)	4.895(0.0020)	0.548		$C_1$	-
18C6•CA-E1	$A_{CA}$	3385, 3407	3372, 3429	35230 (4.369)	4.320(0.0513)	5.041(0.0241)	0.721	10.3	$C_1$	-
18C6•CA-E4	$B_{CA}$	3424	3386, 3396	35548 (4.408)	4.354(0.0554)	4.993(0.0181)	0.639		$C_1$	-

<sup>a</sup> Calculated energies are scaled by 0.8645, 0.8603 and 0.8598 for HQ, RE and CA, respectively, so as to reproduce the observed  $S_1$ - $S_0$  transition of each benzenediol monomer. <sup>b</sup> Ref.53.

Table 2. Relative total energies ( $\Delta E$ [kJ/mol]) of the complexes, interaction energies ( $E_{\text{int}}$ [kJ/mol]), relative energies of the conformers of the 18C6 part ( $\Delta E_{\text{CE}}$ [kJ/mol]) and the benzenediol part ( $\Delta E_{\text{HQ, RE or CA}}$ [kJ/mol]) in the complexes, and dihedral angles of the OH groups of benzenediol in the complexes. The species with bold letters are those experimentally observed. The calculations are performed at the  $\omega$ B97X-D/6-31++G\*\* level.

	18C6-cis-HQ						18C6-RE(III)						18C6-CA							
	$\Delta E$	$E_{\text{int}}$	${}^a \Delta E_{\text{CE}}$	${}^b \Delta E_{\text{HQ}}$	${}^c$ dihedral angle		$\Delta E$	$E_{\text{int}}$	$\Delta E_{\text{CE}}$	$\Delta E_{\text{RE}}$	${}^c$ dihedral angle		$\Delta E$	$E_{\text{int}}$	$\Delta E_{\text{CE}}$	$\Delta E_{\text{CA}}$	${}^c$ dihedral angle			
					${}^a$ OH	${}^b$ OH					${}^a$ OH	${}^b$ OH					${}^a$ OH	${}^b$ OH		
<b>I</b>	<b>0.00</b>	<b>94.3</b>	<b>9.00</b>	<b>1.64</b>	<b>178</b>	<b>178</b>	<b>I</b>	<b>0.00</b>	<b>113</b>	<b>20.0</b>	<b>11.4</b>	<b>178</b>	<b>171</b>	<b>A1</b>	<b>0.00</b>	<b>92.1</b>	<b>10.2</b>	<b>2.28</b>	<b>179</b>	<b>179</b>
II	9.10	88.7	9.26	2.11	168	178	II	1.86	113	17.7	12.2	165	180	<b>E1</b>	<b>3.94</b>	<b>93.2</b>	<b>9.34</b>	<b>7.98</b>	<b>151</b>	<b>160</b>
	-	-	-	-			III	1.97	112	19.1	12.6	167	163	<b>E4</b>	<b>8.66</b>	<b>93.9</b>	<b>7.01</b>	<b>16.2</b>	<b>170</b>	<b>140</b>
	-	-	-	-			IV	3.34	93.7	2.83	10.6	179	179							
	-	-	-	-			V	8.75	91.3	4.13	12.9	158	174		-	-	-	-	-	-

<sup>a</sup>  $\Delta E_{\text{CE}}$  are relative values to that of the most stable 18C6 conformer in the monomer.

<sup>b</sup>  $\Delta E_{\text{HQ, RE or CA}}$  are relative values to the most stable conformer in each benzenediol monomer.

<sup>c</sup> Dihedral angles of  ${}^a$ OH and  ${}^b$ OH are defined in scheme 1.

Scheme 1

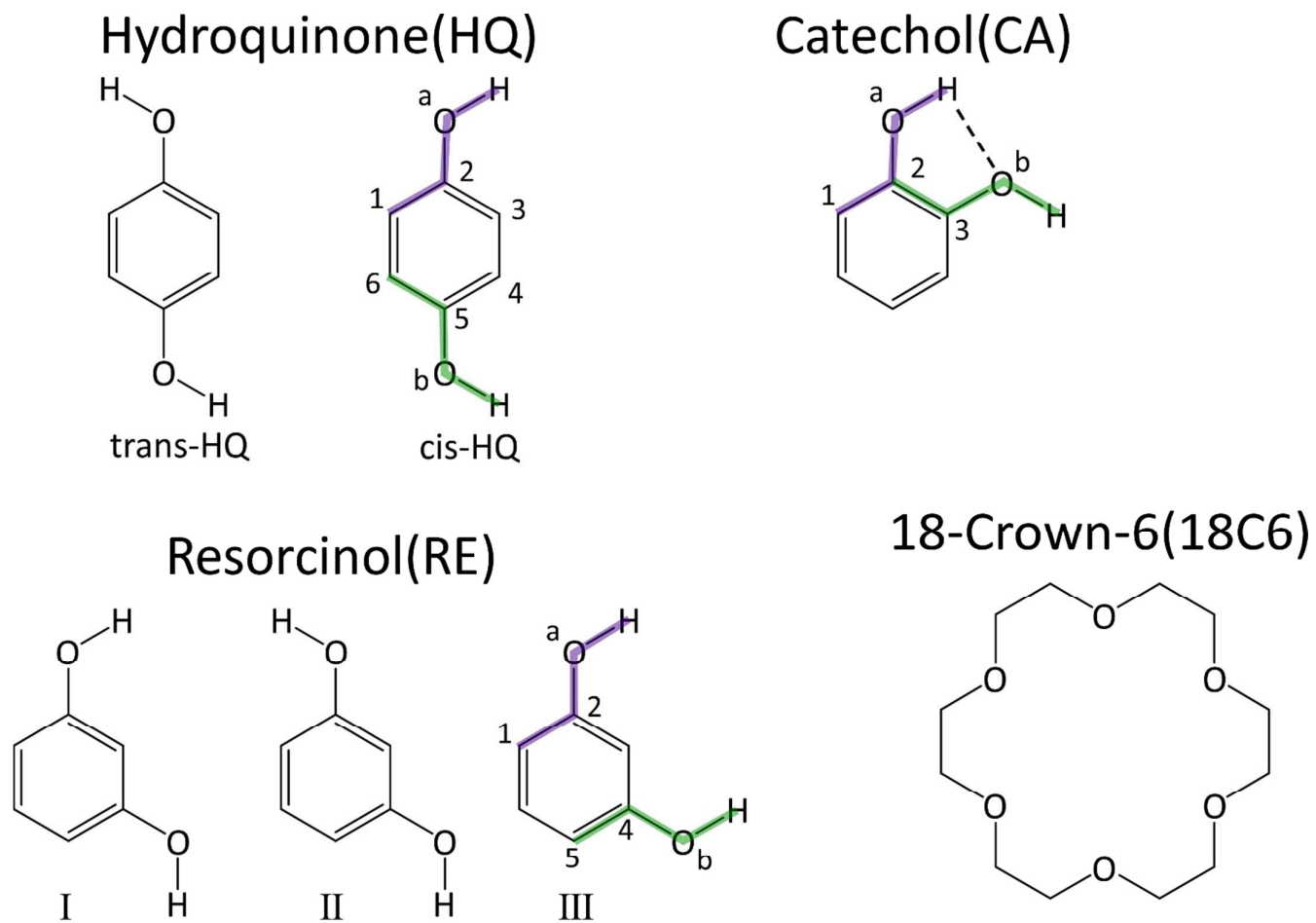




**Figure Caption**

**Fig. 1** The  $S_1$ - $S_0$  LIF spectra of jet-cooled (a) HQ, (b) 18C6•HQ complex, (d) RE, (e) 18C6•RE complex, (g) CA and (h) 18C6•CA complex in the band origin region. (c) and (f) are the UV-UV hole-burning spectra of 18C6•HQ, and 18C6•RE, respectively.

**Fig. 2** (a)-(i) The IR-UV DR spectra of benzenediol monomers and their complexes with 18C6. (j) and (k) The calculated IR spectra of HQ and RE and the complexes with 18C6 at the level of  $\omega$ B97X-D/6-31++G\*\*. In the IR spectra of 18C6•CA complexes, the calculated spectra are shown for comparison. Arrows represent the positions of the OH stretching vibrations of the CA monomer. The calculated IR frequencies are scaled by 0.9346 for CA and its complex, 0.9325 for RE and its complex, and 0.9325 for CA and its complex, in order to reproduce the observed OH stretching vibration of each monomer.

**Fig. 3** Picosecond pump-probe decay profiles of (a)-(c) HQ monomers and 18C6•HQ complex, (d-e) RE monomers and (g) CA monomer. Fluorescence decay curves of (f) 18C6•RE complex and (h), (i) 18C6•CA complexes, obtained with nanosecond laser excitation.

**Fig. 4** (a)(b) Structures of the lowest energy isomers of 18C6•*cis*-HQ within the energy of 10 kJ/mol at the level of  $\omega$ B97X-D/6-31++G\*\* calculation. (c) Structure of 18C6•*trans*-HQ complex, which is ~23 kJ/mol higher than 18C6•*cis*-HQ-I.

**Fig. 5** (a)-(e) Structures of the lowest energy isomers of 18C6•RE(III) within the energy of 10 kJ/mol at the level of  $\omega$ B97X-D/6-31++G\*\* calculation.

**Fig. 6** (a)-(c) Structures of the observed three isomers of the 18C6•CA complexes determined at the level of  $\omega$ B97X-D/6-31++G\*\* calculation.

**Fig. 7** Energy level of 18C6 and benzenediol in most stable conformation in bare forms, that of the distorted ones for forming the complex, and that of the complexes; (a)18C6•HQ and (b)18C6•RE.  $\Delta E_{CE}$ ,  $\Delta E_{HQ}$  and  $\Delta E_{RE}$  represent the destabilization energies due to the distortion of conformation to form the stable complex.  $E_{int}$  represents the interaction energy described in computational section. (see text)

**Fig. 8** Energy level of 18C6 and CA in most stable conformation in bare forms, that of the distorted ones for forming the complex.  $\Delta E_{CE}$  and  $\Delta E_{CA}$  represent the destabilization energy due to the distortion to form the stable host-guest complex.  $E_{int}$  represents the interaction energy described in computational section. (see text)

## Graphic Abstract

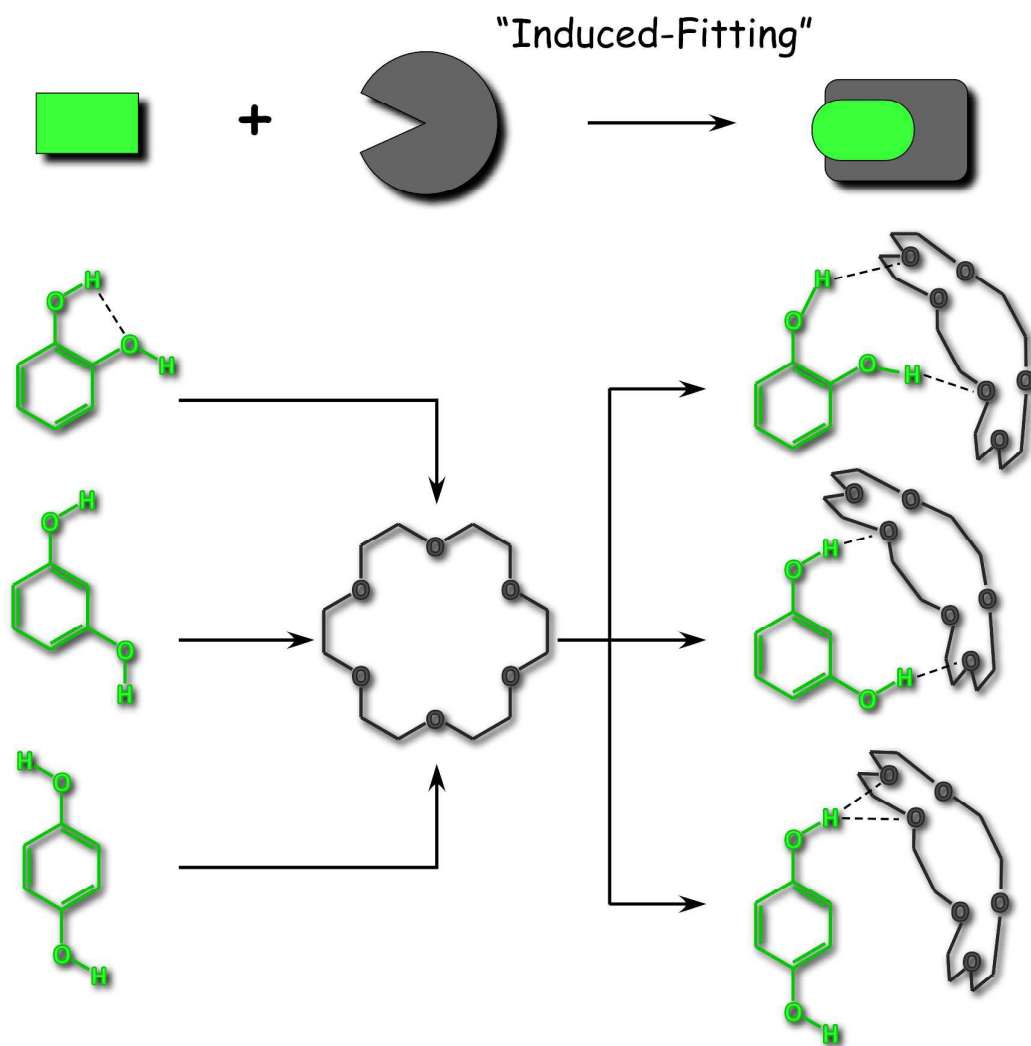


Figure 1

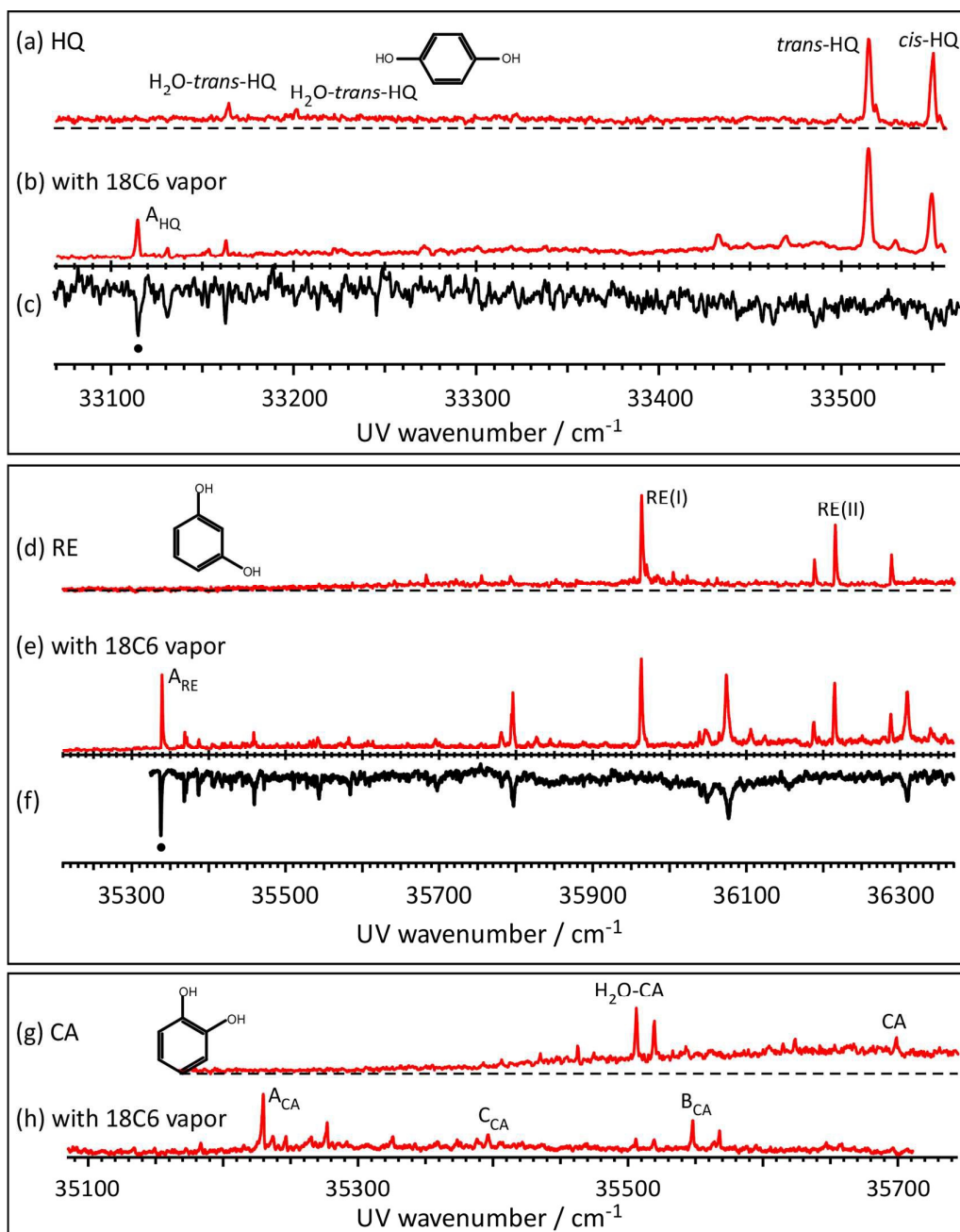


Figure 2

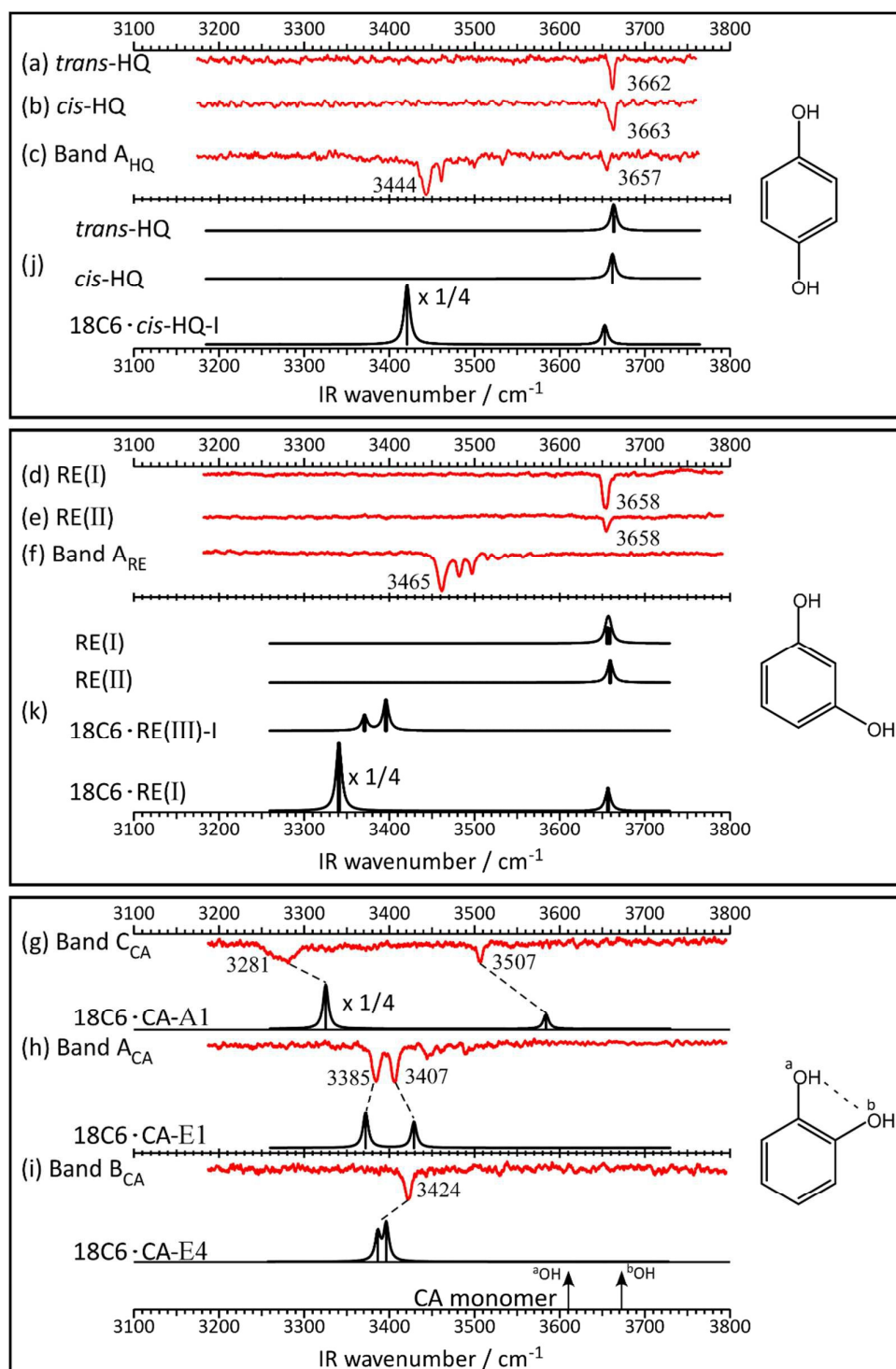


Figure 3

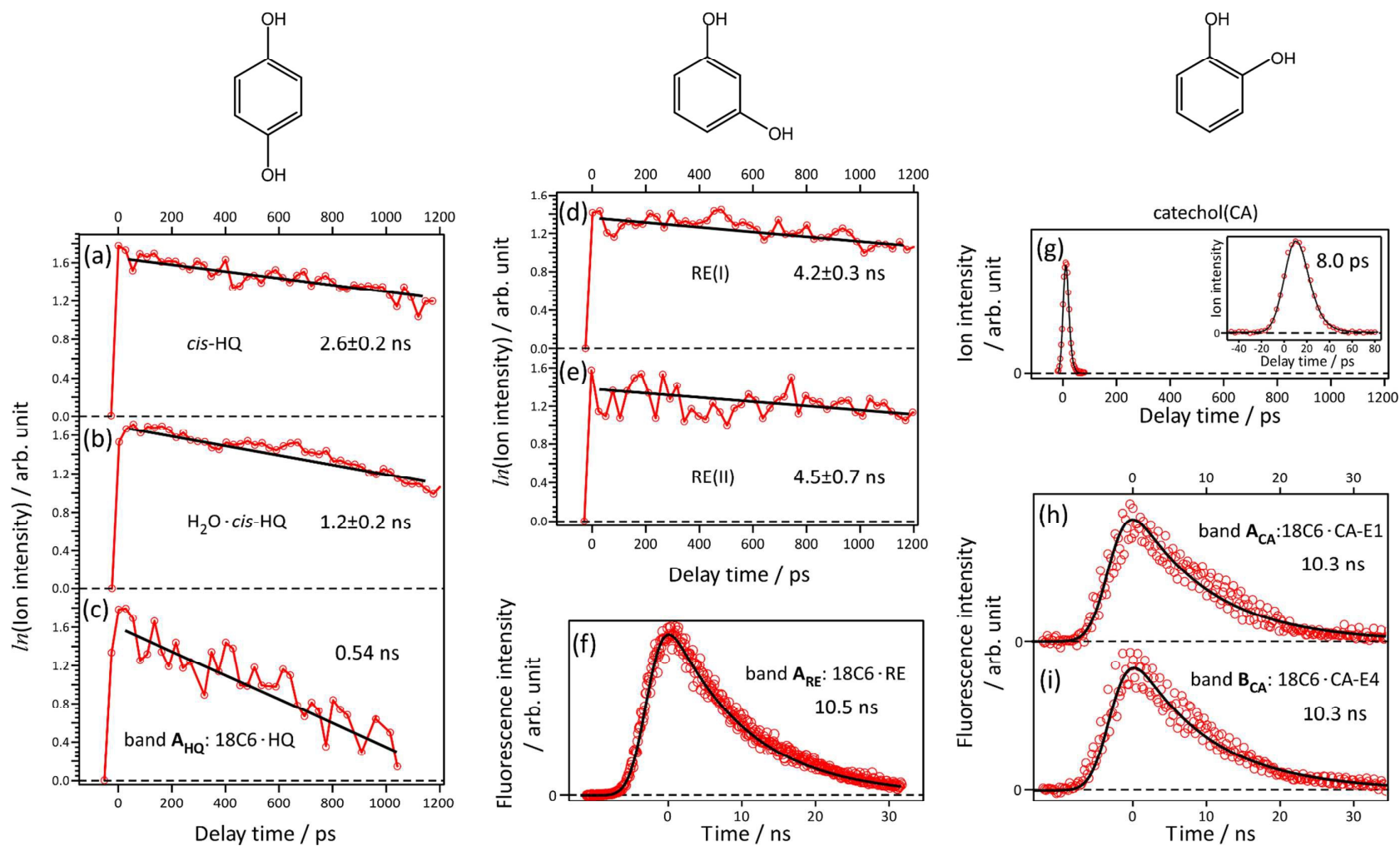


Figure 4

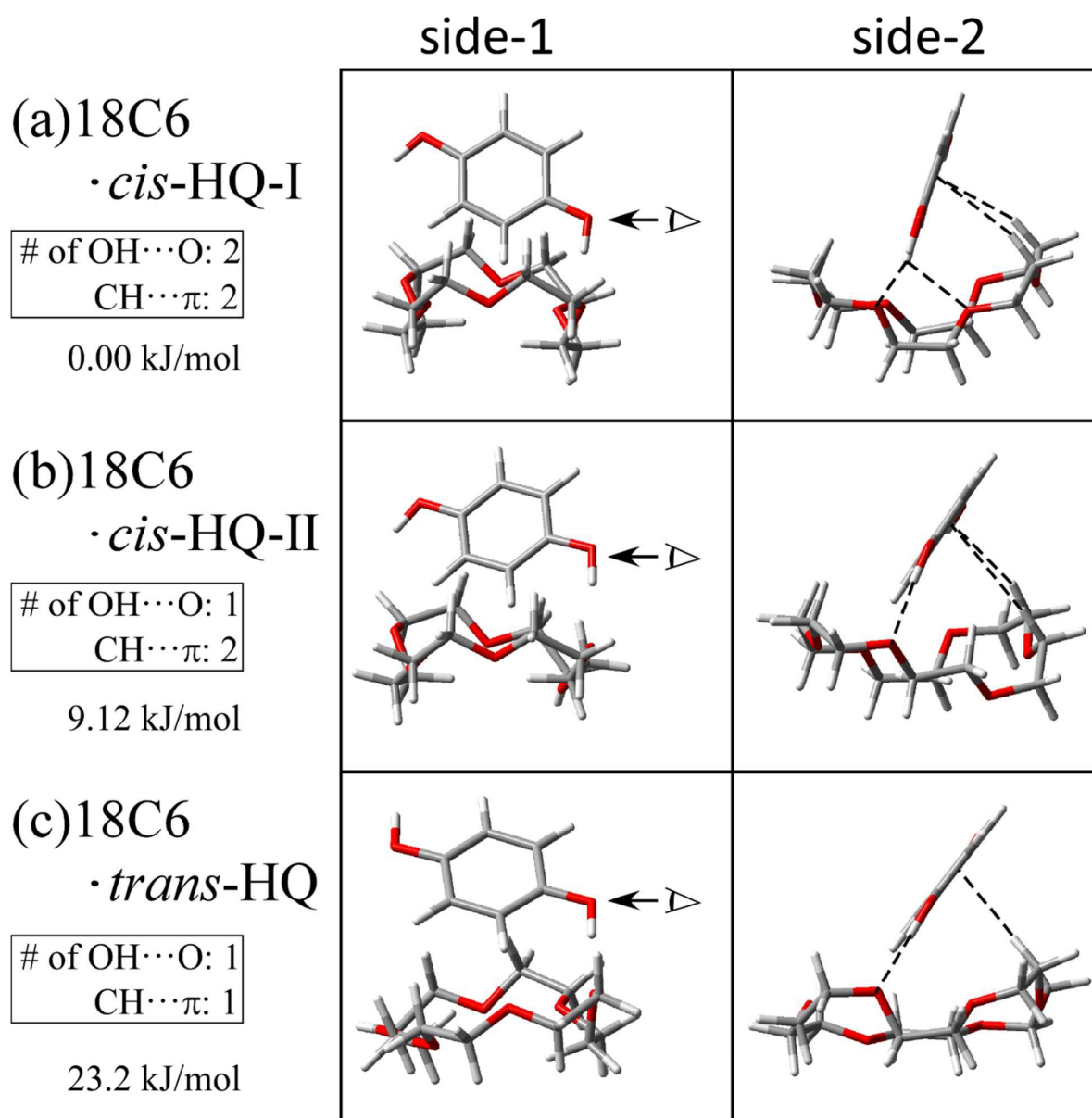


Figure 5

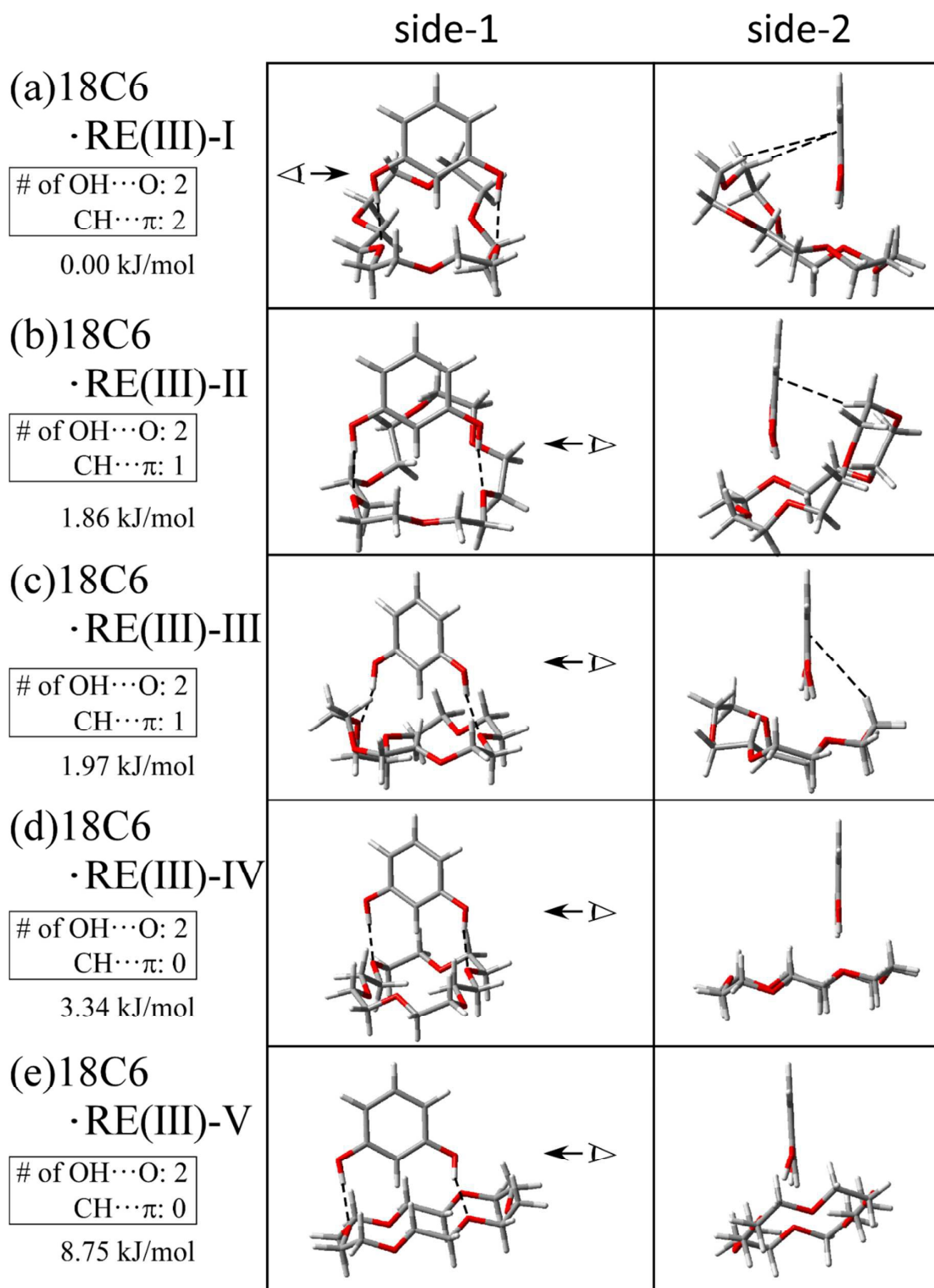




Figure 6

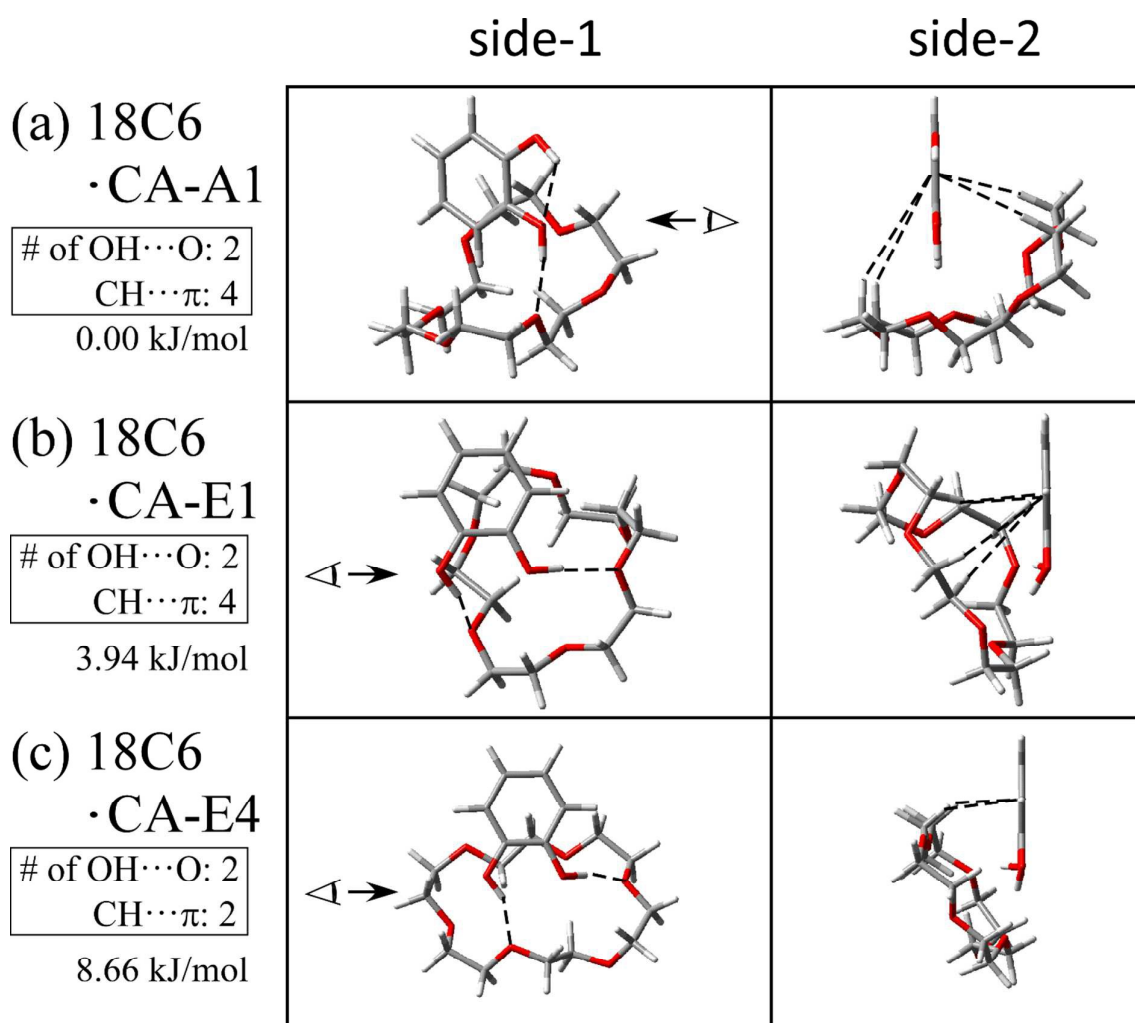


Figure 7

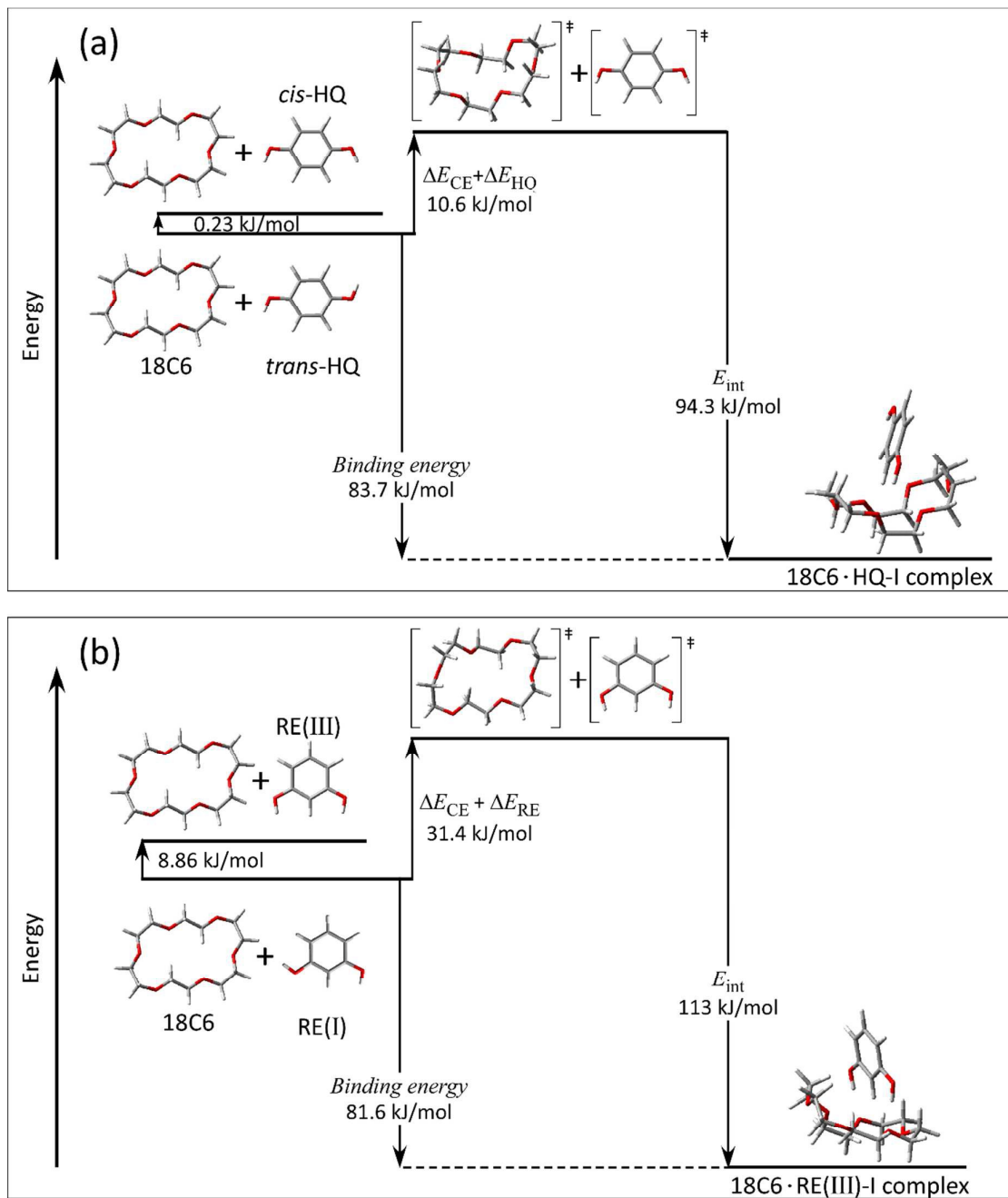


Figure 8

